JTTEE5 14:100-108
DOI: 10.1361/10599630522756
1059-9630/$19.00 © ASM International

Peer Reviewed

# Residual Stress Analysis in Thermally Sprayed Layer Composites, Using the Hole Milling and Drilling Method

*R. Gadow, M.J. Riegert-Escribano, and M. Buchmann*

*(Submitted September 15, 2003; in revised form March 30, 2004)*

**Residual stresses are related to the thermophysical properties of substrate and coating materials and occur after the coated component has undergone thermal spraying and machining processes. All residual stresses in layer composites result from different individual stress mechanisms occurring during the manufacturing process, mainly based on heat and mass transfer during the coating deposition. Using the hole-milling-and-drilling method, residual stress fields can be measured in a quasi-nondestructive way over the drilling depth with appropriate resolution. In several drilling and milling operations, a cylindrically shaped hole is brought step by step into the component surface. The residual stresses are locally relieved due to material removal, deform the surface around the drilled microhole, and are measured by high-resolution measurement tools (e.g., strain gages (DMS)), for every drilling step in the form of relaxed surface strains. Using calibration curves and material data ($E$, $\mu$), the measured surface strains are converted into nominal strains at the bottom of the drilled hole for every drilling step. Out of the differentiated strains, in-plane stress fields can be incrementally determined by Hooke's law. This study describes residual stress measurement features, the finite-element method (FEM) calculation, and the idealization of calibration curves, as well as the results of exemplary stress measurements.**

**Keywords** calibration curves, hole-drilling method, layer composites, residual stresses, thermal spraying

## 1. Introduction

Owing to their cost-effective and flexible processing, as well as to their technical efficiency and operation performance, thermally sprayed layer composites are an important technology in modern surface design and engineering. The determining factor in the operation behavior and functionality of layer composites, especially in tribological and thermomechanical highly loaded operation systems, is the quality and reliability of the composite macrostructure and microstructure. Figure 1 shows the optimization process for thermally sprayed layer composites.

Both aspects are primarily determined by temporary stresses occurring during the manufacturing process and finally by the resulting residual stresses in the layer composites. The influence of temporary and residual stresses on the coating structure and quality can be seen in Fig. 2 to 5.

Residual stresses occur after mechanical, thermal, and chemical processing due to incompatibilities in the elastic and/or elastic-plastic material behavior. Basically, all components contain residual stresses; therefore, during operation a superimposition of arising operation stresses and already existing residual stresses occur. For safety and reliability evaluations as well as for lifetime predictions, both factors must be carefully taken into consideration.

Of great interest are measurement and simulation tools for the determination or prediction of operational and residual stresses in combination with theoretical and experimental stress know-how concerning the influence of stresses on the material and component performance under specific environmental and operation conditions.

## 2. Buildup of Residual Stresses in Thermally Sprayed Layer Composites

During the manufacturing of thermally sprayed layer composites, various stress-generating effects occur that significantly influence the coating and composite quality (Ref 1). The general reasons for stresses in layer composites are different thermal expansions in the composite material caused by temperature gradients and the mismatch in the mechanical and thermophysical properties ($E$, $\mu$, $\alpha$, $\lambda$, $C_p$, and $\rho$) (Ref 2), as well as nonuniform elastic and elastic-plastic deformations in the substrate and coating materials due to thermal or mechanical loading.

Critical stress gradients cause coating failure (e.g., delamination in the coating or interface) (Ref 3), crack networks in the microstructure and macrostructure, plastic material deformation, or a shape distortion of the component. Also, the material properties, yield strength ($R_{P0.01}$) and tensile strength ($R_M$), are positive or negative when superimposed by residual stresses.

The original version of this article was published as part of the ASM Proceedings, *Thermal Spray 2003: Advancing the Science and Applying the Technology*, International Thermal Spray Conference (Orlando, FL), May 5-8, 2003, Basil R. Marple and Christian Moreau, Ed., ASM International, 2003.

**R. Gadow** and **M.J. Riegert-Escribano,** Institute for Manufacturing Technologies of Ceramic Components and Composites, IMTCCC, University of Stuttgart, D-70569 Stuttgart, Germany; and **M. Buchmann,** Federal-Mogul Friedberg GmbH, Engelschalkstrasse 1, D-86316 Friedberg, Germany. Contact e-mail: ifkb@po.uni-stuttgart.de.

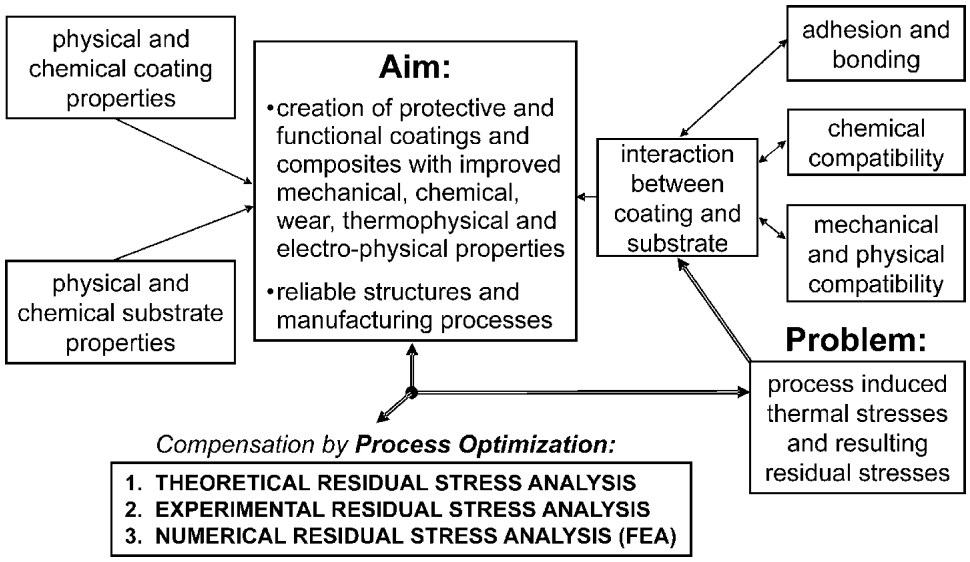


**Fig. 1** Optimization of the functionality and reliability of thermally sprayed layer composites

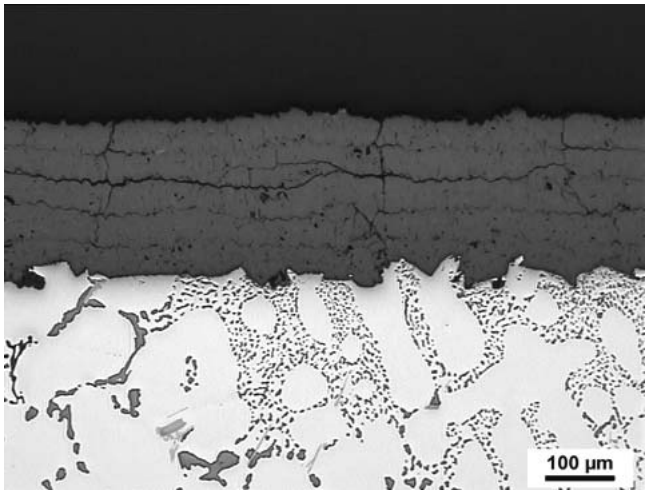


**Fig. 2** Cross section of an APS-sprayed $Cr_2O_3$ coating with a stress-induced crack network

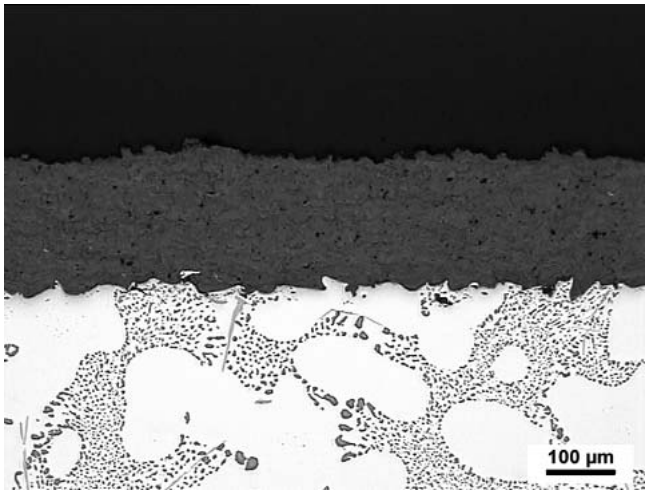


**Fig. 3** Cross section of a stress-optimized and crack-optimized APS-sprayed $Cr_2O_3/TiO_2$ coating

Tensile residual stresses reduce the composite lifetime under dynamic loading, because it favors vertical crack formation and propagation. Also, condensed corrosive products can penetrate the coating through microcracks, can destabilize the coating, and can attack the substrate material. Therefore, tensile stresses in the coating may promote the propagation of stress corrosion cracks. Compressive stresses in the coating increase bonding and alternating fatigue strength (Ref 4, 5).

The final residual stress condition of thermally spray coated components results from several individual stress mechanisms. Figure 6 shows the different stress mechanisms in chronological order.

Substrate preprocessing by grit blasting with corundum of defined particle sizes induces compressive stresses into the substrate surface due to local nonhomogeneous plastic deformations. The size and depth range of the compressive stresses depend on the blasting conditions (i.e., time, distance, and velocity), the used shot (i.e., size and hardness), and finally the blasted components (i.e., geometry, hardness, and deformation behavior).

During thermal spraying, fully or partially molten particles impact on the substrate and subsequent coating layers, flatten, and solidify rapidly. The kinetic energy of the impacting particles induces compressive stresses into the composite material, depending on particle velocity, the percentage of particle fusion, and thermophysical properties. When splats solidify, the contraction, restricted by the substrate material, causes tensile stresses in the single splats. These microscopic stresses in the single splats are relaxed by microcracking. Due to the temperature difference in the layer composite, quenching of the coating takes place. The expansion of the substrate on the one side and the contraction of the coating on the other side additionally in-

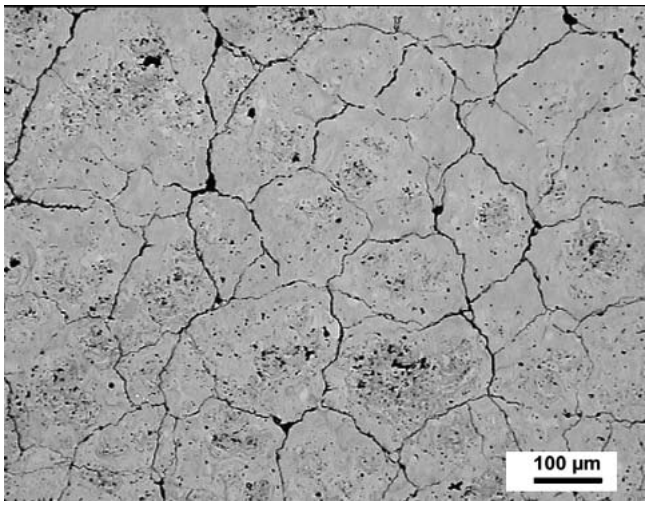


**Fig. 4** Surface section of an APS-sprayed $TiO_2$ coating with a stress-induced crack network

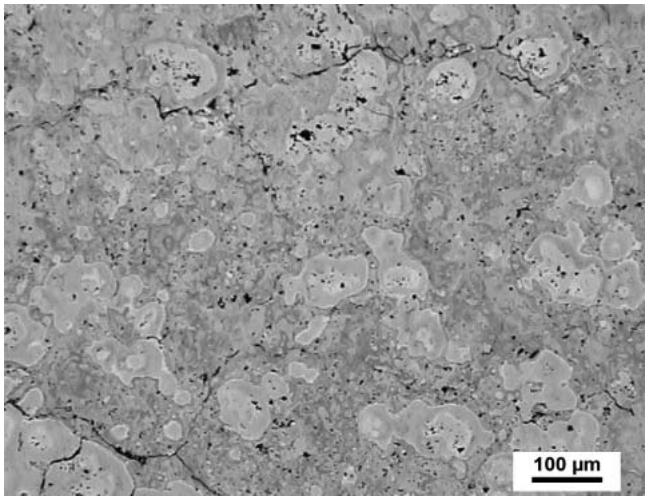


**Fig. 5** Surface section of a stress-optimized and crack-optimized APS $TiO_2$ coating

duce macroscopic tensile stresses, so-called *quenching stresses*, into the coating. After temperature compensation between the substrate and coating, thermal stresses arise during subsequent cooling (Ref 6). The mismatch in the thermophysical material properties, mainly the differences in the thermal expansion coefficients, result in tensile stresses for $\alpha_{coating} > \alpha_{substrate}$ and in compressive stresses for $\alpha_{coating} < \alpha_{substrate}$. The absolute macroscopic stress values depend on the Young's modulus $E_{C/S}$ ratio, where $E_C$ is reduced by the coating porosity. To realize the defined surface qualities, different mechanical processing steps (e.g., grinding, polishing, and lapping) or thermal processing steps are performed. These induce stress peaks, which superimpose and change the residual stress situation of the whole composite (Ref 7, 8). Figure 7 displays finite-element method (FEM)-calculated, time-dependent stresses during an APS coating process of a $TiO_2$-$AlMg_3$ layer composite (i.e., coating, interface, and substrate).

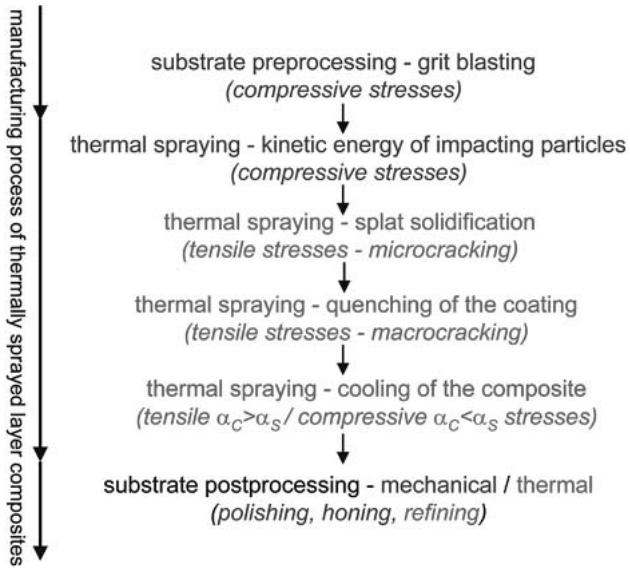


**Fig. 6** Individual stress mechanisms during thermal spraying

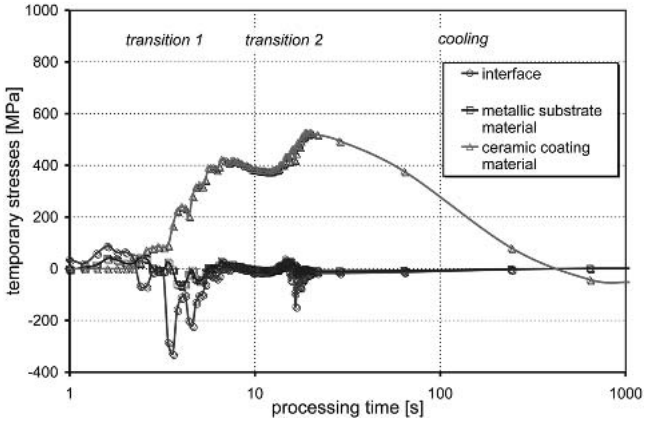


**Fig. 7** Calculated stress distribution during APS spraying (Ref 9)

## 3. Hole Drilling and Milling Method

Residual stresses can be measured by various techniques, which basically are classified into destructive or partially destructive mechanical methods and nondestructive physical methods (i.e., acoustic, optic, and diffraction (x-ray and neutron)). Decisive factors for the selection of an individual measurement technique are depth range and accuracy, cost and time exposure, reproducibility, geometry, and material dependence.

In recent years, a new mechanical technique, the advanced incremental drilling-and-milling method, became more and more important for the determination of residual stresses in components. The main advantages of this technology are the independence of the component geometry, the possibility of in situ measurements, the determination of residual stress depth profiles up to several millimeters, and its quasi-nondestructive character (Ref 10-12). The relatively small holes can be filled afterward by point welding or galvanic tampon deposition.

In several drilling-and-milling processes, a cylindrically

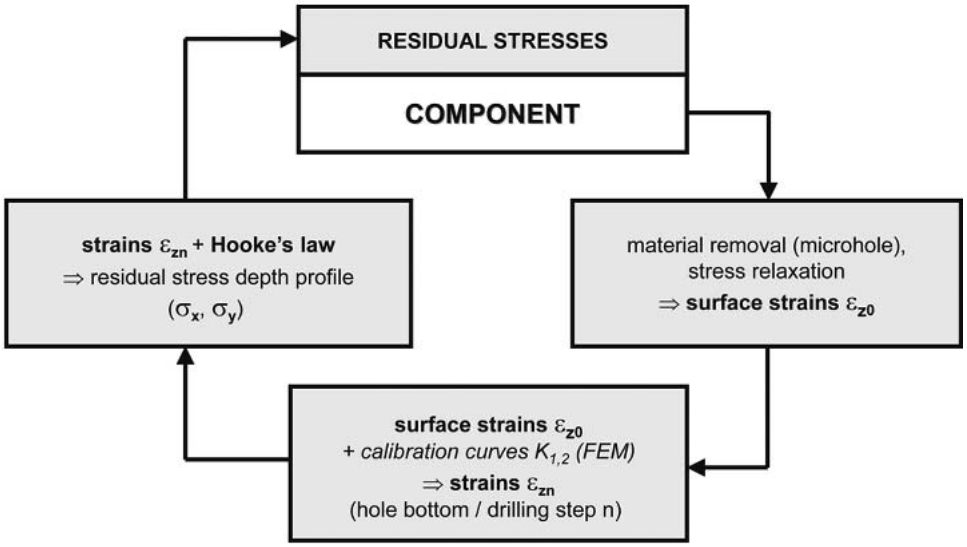


**Fig. 8** Processing scheme for the determination of residual stresses using the hole-drilling method

shaped hole, typically with a hole diameter of between 1.0 and 1.8 mm (diameter of the drill tip 0.9 mm), is brought stepwise (~5-20 μm) into the component surface. The stepping motors are computer-controlled via personal computer. The combination of high-speed drilling (300,000 rpm) and low penetration rate (~60 μm/min) in addition with a small drilling depth per drilling step guarantees a stress-free drilling process with negligible heat development, even in extremely hard materials. For the machining of the component surface, diamond drilling tools are used having either diamond particles embedded into a galvanic deposited NiCr coating or a hard alloy drilling tool that is coated with PVD or CVD with a TiN, TiC, or DLC coating (Ref 13).

The residual stresses in the layer composite are locally relieved due to the material removal, deform the surface around the microhole, and are measured using strain gages (DMS) for every drilling step as relaxed surface strains $\varepsilon_{z0}$. The strain gages consist of three single-measurement grids, which are arranged radially under an exact defined angle around the drilled hole. By using calibration curves in longitudinal and transverse directions $K_{1,2}(z_n)$ and material properties ($E$, μ), the measured surface strains $\varepsilon_{z0}$ are converted to nominal strains $\varepsilon_{zn}$ at the bottom of the hole for every drilling step $z_n$. Out of the strain gradients $d\varepsilon(z)/dz$, in-plane stress fields $\sigma(z)$ are incrementally determined via Hooke's law for every drilling depth $z_n$. Figure 8 shows the general process scheme for hole-drilling measurements.

A schematic drawing of the drilling-and-milling process is shown in Fig. 9, where $R$ represents the gage circle radius, which is characteristic for each strain gage type, and $D_o$ is the diameter of the drilled hole.

Considering the investigated surface as a sector of an $x$-$y$-plane, it can be assumed that the $z$-direction is stress free. In the case of a two-axis ($x$-$y$) elastic stress field, incremental strain rates can be recorded by the strain gage in the grid direction for every drilling step. The measured surface strains in the grid direction are due to longitudinal and superimposed transverse stresses, which are relieved by material removal. Figure 10 illustrates the nomenclature of the strain orientations.

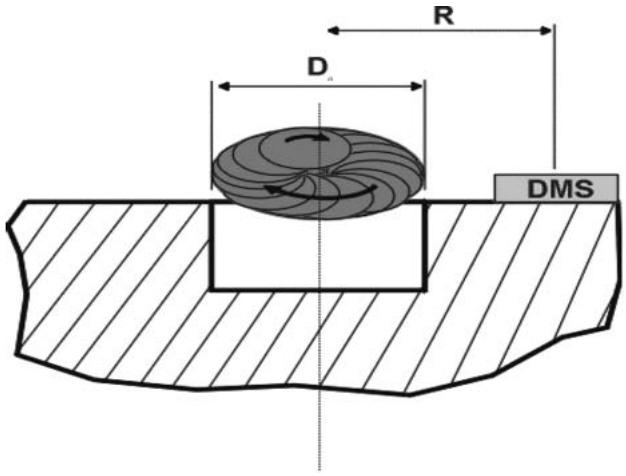


**Fig. 9** Combination of drilling and milling processes

The correlation between the measured incremental surface strain rate $d\varepsilon(z)/dz$ and the nominal strains $\varepsilon_n(z)$ at the bottom of the drilled microhole are made via calibration curves $K_{1,2}$, with $K_1$ in the longitudinal direction and $K_2$ in the transverse direction (Eq 1-3). The subscripts 0, 45, and 90 refer to the three measured grid directions.

$$d\varepsilon_0(z)/dz = K_1(z) \cdot \varepsilon_{n0}(z) - K_2(z) \cdot \mu \cdot \varepsilon_{n90}(z) \quad \text{(Eq 1)}$$

$$d\varepsilon_{45}(z)/dz = K_1(z) \cdot \varepsilon_{n45}(z) - K_2(z) \cdot \mu \cdot [\varepsilon_{n0}(z) + \varepsilon_{n90}(z) - \varepsilon_{n45}(z)] \quad \text{(Eq 2)}$$

$$d\varepsilon_{90}(z)/dz = K_1(z) \cdot \varepsilon_{n90}(z) - K_2(z) \cdot \mu \cdot \varepsilon_{n45}(z) \quad \text{(Eq 3)}$$

Per definition, the calibration curves must be stress-independent and material-independent. Due to the precise grid positions, the in-plane strain field is exactly defined, and the variable strain

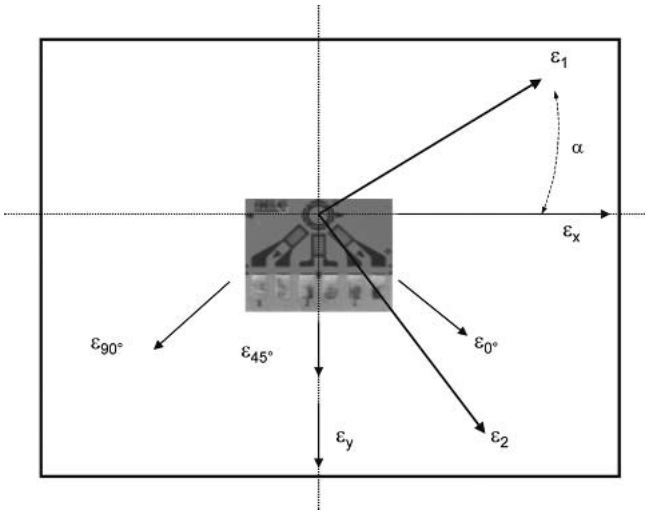


**Fig. 10** Nomenclature of the strain directions on an investigated plane plate

directions and rates can be determined. Out of the longitudinal strains in the individual grid direction the longitudinal stresses can be calculated using Hooke's law (Eq 4-6):

$$\sigma_0(z) = \frac{E}{K_1^2(z) - \mu^2 \cdot K_2^2(z)} \cdot \left[ K_1(z) \cdot \frac{d\varepsilon_0(z)}{dz} + \mu \cdot K_2(z) \cdot \frac{d\varepsilon_{90}(z)}{dz} \right] \quad \text{(Eq 4)}$$

$$\sigma_{45}(z) = \frac{E}{K_1^2(z) - \mu^2 \cdot K_2^2(z)} \cdot \left[ K_1(z) \cdot \frac{d\varepsilon_{45}(z)}{dz} + \mu \cdot K_2(z) \cdot \frac{d\varepsilon_0(z) + d\varepsilon_{90}(z) - d\varepsilon_{45}(z)}{dz} \right] \quad \text{(Eq 5)}$$

$$\sigma_{90}(z) = \frac{E}{K_1^2(z) - \mu^2 \cdot K_2^2(z)} \cdot \left[ K_1(z) \cdot \frac{d\varepsilon_{90}(z)}{dz} + \mu \cdot K_2(z) \cdot \frac{d\varepsilon_0(z)}{dz} \right] \quad \text{(Eq 6)}$$

Due to the exactly defined grid arrangement, the principal stresses ($\sigma_1$, $\sigma_2$) as well as the variably oriented stresses (e.g., $\sigma_x$ and $\sigma_y$) can be analyzed using Eq 7 and 8.

$$\sigma_{1,2}(z) = \frac{\sigma_0(z) + \sigma_{90}(z)}{2} \pm \frac{1}{\sqrt{2}} \cdot \sqrt{(\sigma_0(z) - \sigma_{45}(z))^2 + (\sigma_{90}(z) - \sigma_{45}(z))^2} \quad \text{(Eq 7)}$$

$$\sigma_{x,y}(z) = \frac{\sigma_1(z) + \sigma_2(z)}{2} \pm \frac{\sigma_1(z) - \sigma_2(z)}{2} \cdot \cos 2\,(\alpha - 45) \quad \text{(Eq 8)}$$

Figures 11 and 12 show the influence of different Young's moduli $E_{C/S}$ ratios (coating/substrate) on the calculated calibration curves. The calibration curves $K_{1,2}$ are determined by numerical FEM calculations (Ref 14, 15).

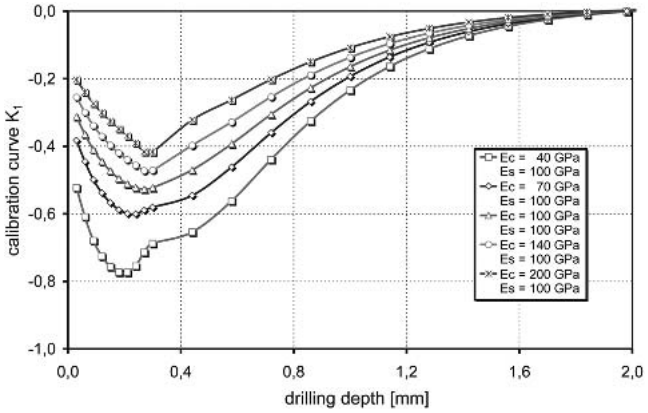


**Fig. 11** Calibration curve $K_1$ as a function of Young's moduli $E_{C/S}$ ratios, with a coating thickness of 200 μm

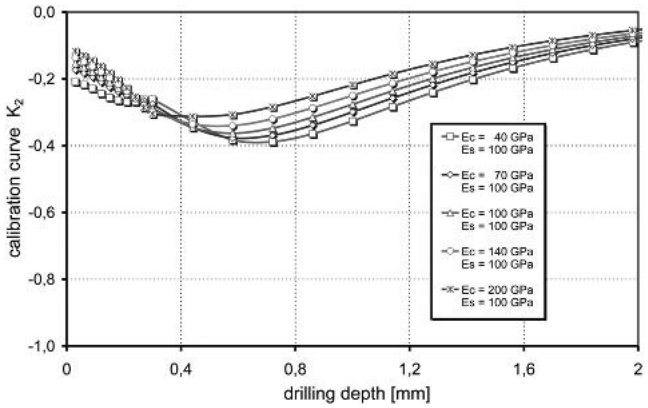


**Fig. 12** Calibration curve $K_2$ as a function of Young's moduli $E_{C/S}$ ratios, with a coating thickness of 200 μm

The measurement data and individual calculation steps are well demonstrated in the following figures for a grit-blasted (6 bar) aluminum plate ($E$ = 70 GPa; $\mu$ = 0.33). The measured strains ($\varepsilon_0$, $\varepsilon_{45}$, and $\varepsilon_{90}$) and calculated stresses ($\sigma_1$, $\sigma_2$, $\sigma_x$, and $\sigma_y$) up to a drilling depth of 0.6 mm are shown in Fig. 13 and 14.

The strain gradients indicate the kind and size of existing residual stresses. For positive and negative strain gradients, compressive and tensile stresses, respectively, can be expected. Higher stresses are characterized by larger strain gradients.

The calculated in-plane stresses in the grit-blasted aluminum plate are more or less identical for all calculated stress directions. This is a typical result for residual stress fields in grit-blasted surfaces as well as in thermally sprayed layer composites. Therefore, the measured stress fields of the investigated substrate materials and layer composites can be well characterized by one stress depth profile.

## 4. Residual Stresses in Grit-Blasted Substrate Materials

The adhesion between the substrate and coating material is based on a mechanical bonding mechanism. To improve the

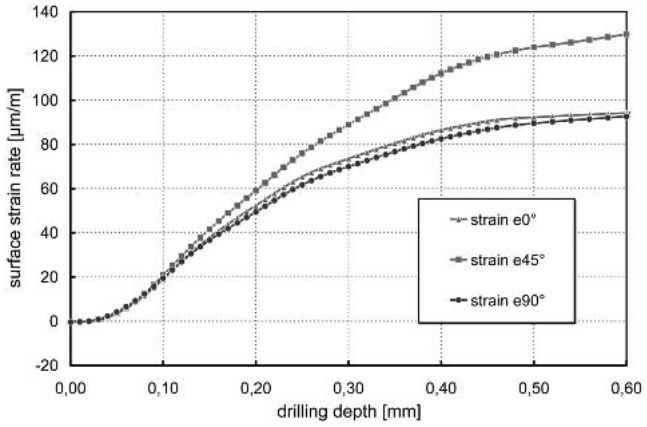


**Fig. 13** Measured strain signals for the different grid directions ($\varepsilon_{0°}$, $\varepsilon_{45°}$, $\varepsilon_{90°}$)

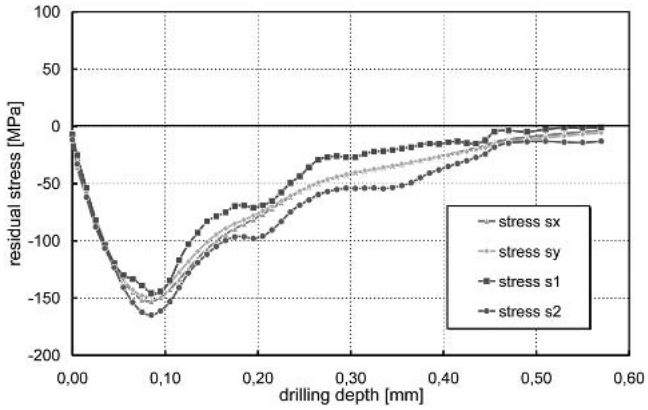


**Fig. 14** Calculated principal residual stresses ($\sigma_1$ and $\sigma_2$) and stresses in the *x*-direction and *y*-direction ($\sigma_x$ and $\sigma_y$, respectively)

coating adhesion, the substrate surface is roughened (activated) by grit blasting to enlarge the specific substrate surface. Besides the roughening effect, grit blasting induces compressive residual stresses into the substrate surface, due to elastic-plastic interactions between the blasting shot and the substrate surface. The compressive stresses reinforce the substrate surface, while the substrate hardness increases locally.

In a first test, the residual stresses and surface hardness of grit-blasted AlSi9 substrate materials were investigated. Due to the homogeneous stress field (in-plane) the residual stresses can be well defined by a single stress depth distribution. The grit-blasting process (EK36, noble white corundum particles; size 0.42-0.60 µm) was performed with a blasting distance of 50 mm and a feed drive of 5 mm/s. The blasting pressure was varied between 2 and 6 bar. Figures 15 and 16 show the measured residual stress and hardness depth profiles, starting on the substrate surface.

As expected, grit blasting induces compressive stresses into the substrate surface. The compressive stress size and depth increase with increasing blasting pressure. A maximum compressive stress level of 150 MPa was evaluated for a blasting pressure of 6 bar directly below the substrate surface. The AlSi9 surface hardness increases with increasing compressive stresses.

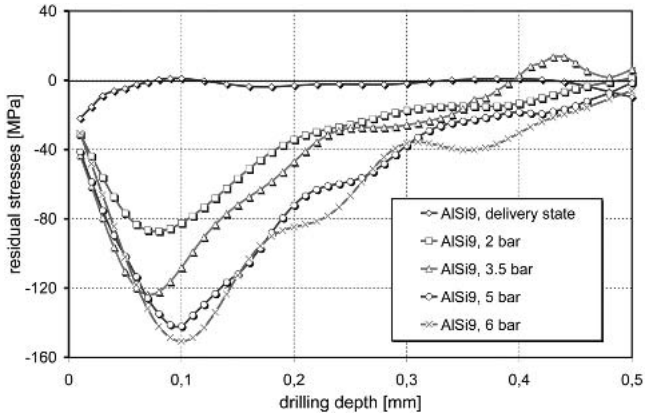


**Fig. 15** Measured residual stresses in grit-blasted AlSi9 substrate materials, with variations in blasting air pressure

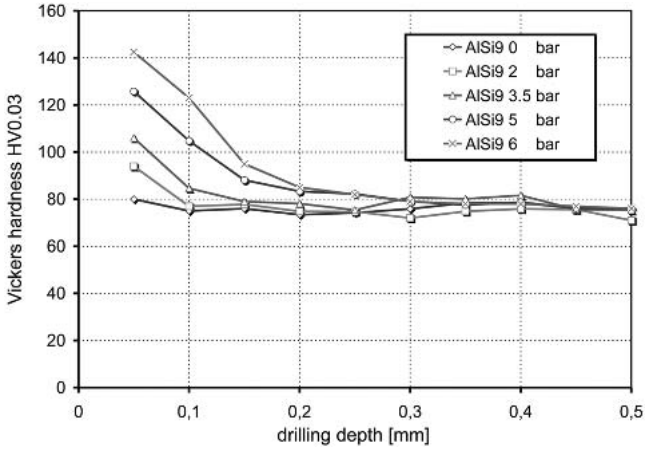


**Fig. 16** Measured Vickers hardness $HV_{0.03}$ in grit-blasted AlSi9 substrate materials, with variations in blasting air pressure

For a blasting pressure of 6 bar, the surface hardness (~140 $HV_{0.03}$) is almost twice as great as that of the untreated surface (~80 $HV_{0.03}$).

In a second test, the residual stresses in different substrate materials (e.g., magnesium alloy AM50, aluminum alloy AlSi9, titanium alloy Ti4, and steel alloy St42), which were grit-blasted with a constant blasting pressure of 6 bar, were investigated (Fig. 17).

The residual stresses in the substrate surface increase proportionally with increasing the Young's modulus of the substrate material. The highest compressive residual stresses (~300 MPa) were measured in the St42 substrate material.

## 5. Residual Stresses in Thermally Sprayed Layer Composites

The residual stresses in thermally sprayed layer composites are mainly influenced by material combinations with different properties, processing parameters (temperature and kinetic energy), and cooling processes. In this study, residual stress inves-

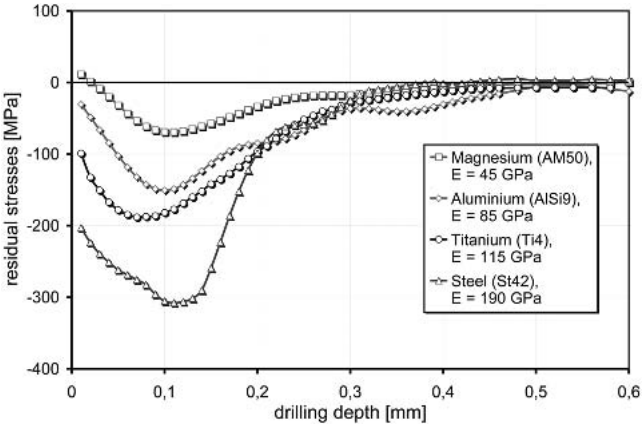


**Fig. 17** Measured residual stresses in different grit-blasted substrate materials

tigations were performed on APS-sprayed (with different hydrogen mass flow rates) and HVOF-sprayed (propane and kerosene) FeCr17 coatings on AlSi substrate materials (Fig. 18-21). For the calculation of the calibration curves, a Poisson's ratio of $\mu = 0.28$ for all of the coatings was assumed (influence of <2% in the calibration coefficients in the case of a blind hole) (Ref 16). The Young's modulus was determined by surface acoustic wave measurements. For the APS-sprayed and HVOF-sprayed FeCr17 coatings, Young's moduli of 75 and 118 GPa, respectively, were measured. The measured Young's modulus of the aluminum substrate was 75 GPa (Ref 14, 17).

The residual stresses were measured to a depth of 0.6 mm, as shown in Fig. 22. The different FeCr17-AlSi composites have a homogeneous coating thickness of 250 µm.

In both HVOF-sprayed coatings, compressive stresses were determined. The compressive stresses increased with increasing kinetic energy. In the HVOF kerosene-sprayed FeCr17 coating, compressive stresses up to 150 MPa were measured. The APS-sprayed coatings indicate tensile stresses. With increasing hydrogen mass flow, which means higher process temperatures, the tensile stresses in the FeCr17 coating increase.

The influence of residual stresses on coating hardness and adhesion can be seen in Fig. 23 and 24. The hardness investigations were carried out using a universal hardness-measuring machine (Fischerscope HCU). The microindentation tests with a Vickers indenter were performed on metallographically polished cross sections.

The adhesion of the coating was measured using a Zwick Z100 universal mechanical testing machine. A steel tension rod is glued on the coating surface, and the tensile load is continuously increased. As soon as the delamination of the coating occurs, the tensile load is measured and the bonding strength is determined.

The coating hardness and adhesion of HVOF-sprayed FeCr17 coatings are higher than those of APS-sprayed coatings. Both coating characteristics increase with increasing compressive residual stresses in the coating material.

## 6. Summary and Conclusions

Residual stresses induced by thermal spraying have a great influence on the properties and operation lifetime of layer composites. This is of importance whenever materials with distinctly different thermophysical properties are combined. Reliable measurement tools are a key requirement for an optimized and reliable manufacturing process and for successful engineering in product development. The advanced hole-drilling-and-milling method is a very convenient method to determine residual stresses and their gradients in layer composites over the drilling depth. The combination of a drilling-and-milling movement provides advantages compared with conventional drilling methods in terms of lower generated stresses near the drilled hole, and avoiding errors in the residual stress measurements due to plasticity, and undesired local heating.

Using FEM-calculated calibration curves, the residual stresses of layer composites with inhomogeneous mechanical material properties can be determined.

The relationships between composite properties, such as bonding strength and hardness, and the residual stress depth profile were investigated.

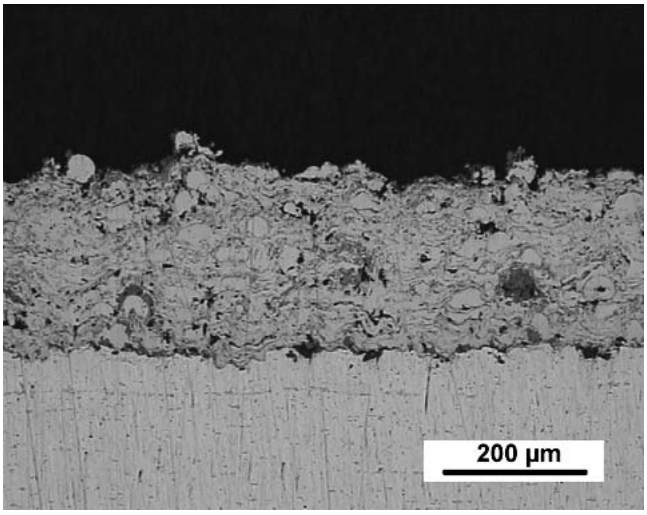


**Fig. 18** APS-sprayed FeCr17 coating (a: 8 L/min $H_2$)

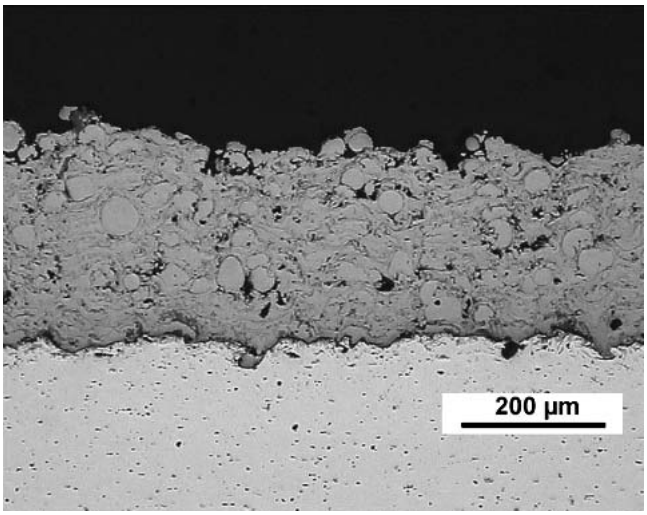


**Fig. 19** APS-sprayed FeCr17 coating (b: 4 L/min $H_2$)

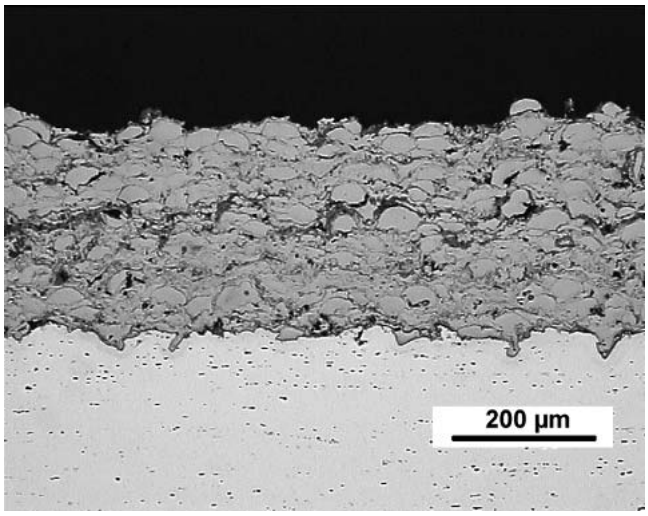


**Fig. 20** HVOF (propane)-sprayed FeCr17 coating

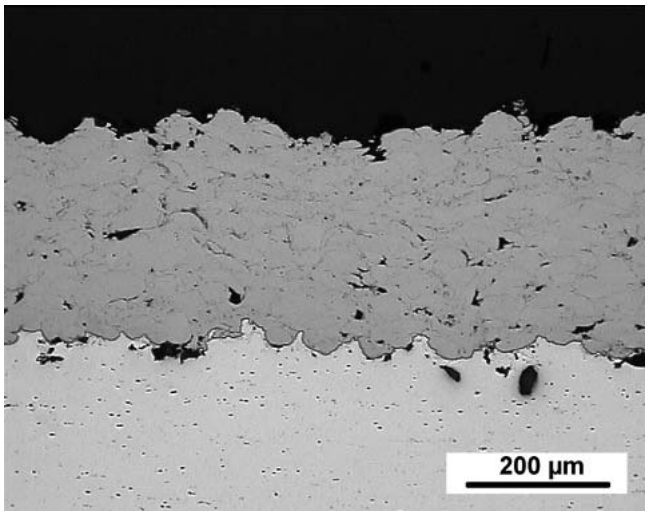


**Fig. 21** HVOF (kerosene)-sprayed FeCr17 coating

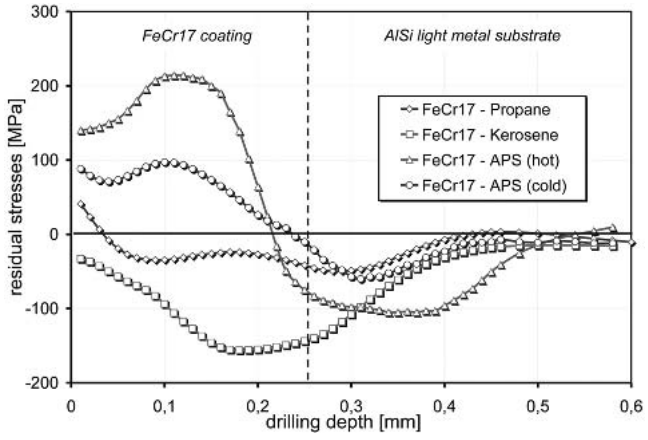


**Fig. 22** Measured residual stresses in FeCr17-AlSi layer composites

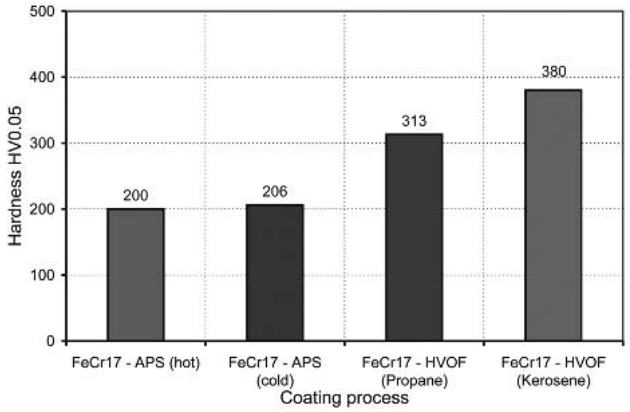


**Fig. 23** Measured FeCr17 coating hardness ($HV_{0.05}$)

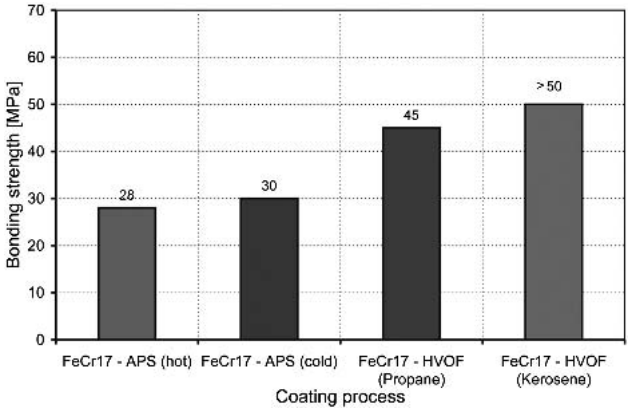


**Fig. 24** Measured FeCr17 coating adhesion

The grit-blasting process induces compressive stresses into the material surface, and an increase in the surface hardness was measured. For a given blasting pressure, the highest compressive stresses were measured for the material with the highest Young's modulus.

In this work, the HVOF technology led to layer composites with a higher bonding strength and hardness compared with APS-sprayed coatings. For the HVOF-sprayed FeCr17 coatings, compressive stresses were measured, which were the opposite of the APS-sprayed coatings, under a tensile stress state.

## References


1. K.A. Khor and Y.W. Gu, Effects of Residual Stresses on the Performance of Plasma Sprayed Functionally Graded $ZrO_2$/NiCoCrAlY Coatings, *Mater. Sci. Eng., A,* Vol 277, 2000, p 64-76
2. K.A. Khor, Y.W. Gu, and Z.L. Dong, Plasma Spraying of Functionally Graded $ZrO_2$/NiCoCrAlY coating System Using Composite Powders, *Thermal Spray: Meeting the Challenges of the 21st Century,* C. Coddet, Ed., May 25-29, 1998 (Nice, France), ASM International, 1998, p 1543-1549
3. T.W. Clyne and S.C. Gill, Residual Stresses in Thermal Spray Coatings and their Effect on Interfacial Adhesion: A Review of Recent Work, *J. Thermal Spray Technol.,* Vol 5 (No. 4), 1996, p 401-418
4. R.T.R. McGrann, D.J. Greving, E.F. Rybicki, J.R. Shadley, D.A. Som-

merville, and B.E. Bodger, Fatigue Life in Bending and Coating Residual Stress in Tungsten Carbide Thermal Spray Coatings on Aluminum and Steel Substrates, *Thermal Spray: A United Forum for Scientific and Technological Advances,* C.C. Berndt, Ed., Sept 15-18, 1997 (Indianapolis, IN), ASM International, 1997, p 737-742
5. L. Pejryd, J. Wigren, D.J. Greving, J.R. Shadley, and E.F. Rybicki, Residual Stress as a Factor in the Selection of Tungsten Carbide Coatings for a Jet Engine Application, *J. Thermal Spray Technol.,* Vol 10 (No. 3), 2001, p 268-274
6. L. Pawlowski, *The Science and Engineering of Thermal Spray Coatings,* John Wiley & Sons, Chichester, U.K., 1995
7. S. Kuroda, Properties and Characterization of Thermal Sprayed Coatings: A Review of Recent Research Progress, *Thermal Spray: Meeting the Challenges of the 21st Century,* C. Coddet, Ed., May 25-29, 1998 (Nice, France), ASM International, p 539-551
8. B. Scholtes, *Eigenspannungen in mechanisch randschichtverformten Werkstoffzuständen: Ursachen, Ermittlung und Bewertung* (*Residual Stresses in Mechanically Surface Deformed Material Conditions: Reasons, Determination and Evaluation*), DGM-Informationsges, 1991 (in German)
9. M. Buchmann and R. Gadow, Estimation of Residual Stresses from the Simulation of the Deposition Process of Ceramic Coatings on Light Metal Cylinder Liners, *Ceram. Eng. Sci. Proc.,* Vol 3 (No. 22), 2001, p 329-336
10. M. Buchmann and R. Gadow, High Speed Circular Microhole Milling Method for the Determination of Residual Stresses in Coatings and Composites, *Ceram. Eng. Sci. Proc.,* Vol 3 (No. 21), 2000, p 109-116
11. T. Schwarz, "Beitrag zur Eigenspannungsermittlung an isotropen, anisotropen sowie inhomogenen, schichtweise aufgebauten Werkstoffen mittels Bohrlochmethode und Ringkernverfahren" ("Residual Stress Measurement in Isotropic, Anisotropic and Inhomogeneous Layer Composites Using the Hole Drilling and Ringcore Drilling Method"), Ph.D. dissertation, MPA University of Stuttgart, 1996 (in German)
12. F. Haase, *Eigenspannungsermittlung an dünnwandigen Bauteilen und Schichtverbunden* (*Residual Stress Analysis in Thin-Walled Components and Layer Composites*), Shaker Verlag GmbH, Aachen, Germany, 1998, (in German)
13. M. Buchmann, C Friedrich, and R. Gadow, Residual Stress Characterization of Thermal Barrier Coatings: Comparison of Thermally Sprayed, EB-PVD and CVD Based Coatings, *Ceram. Eng Sci. Proc.,* Vol 4 (No. 21), 2000, p 663-670
14. M. Escribano, "Determination of the Young's Moduli and Residual Stresses of Thermally Sprayed Layer Composites," Diploma thesis, Institute for Manufacturing Technologies of Ceramic Components and Composites, University of Stuttgart, 2001
15. M. Buchmann and R. Gadow, High Speed Circular Microhole Milling Method for the Determination of Residual Stresses in Coatings and Composites, *Ceram. Eng. Sci. Proc.,* Vol. 3 (No. 21), 2000, p 109-116
16. G.S. Schajer, Application of Finite Element Calculations to Residual Stress Measurements, *J. Eng. Mater. Technol.,* Vol 103, 1981, p 157-163
17. M. Buchmann, G. Bürkle, M. Escribano, H.-J. Fecht, R. Gadow, and M. Mahlich, On the Elastic Mechanical Properties of Thermally Sprayed Coatings, *International Thermal Spray: Conference,* E. Lugscheider and C.C. Berndt, Ed., March 4-6, 2002 (Essen, Germany), DVS Deutscher Verband für Schweißen, 2002, p 598-605